Structural Studies of *Streptococcus pyogenes* Streptolysin O Provide Insights into the Early Steps of Membrane Penetration

Susanne C. Feil[1]**, David B. Ascher**[1]**, Michael J. Kuiper**[2]**, Rodney K. Tweten**[3]** and Michael W. Parker**[1,4]

1 - ACRF Rational Drug Discovery Centre, Biota Structural Biology Laboratory, St. Vincent's Institute of Medical Research, Fitzroy, Victoria 3065, Australia
2 - Victorian Life Sciences Computation Initiative, The University of Melbourne, Parkville, Victoria 3010, Australia
3 - Department of Microbiology and Immunology, University of Oklahoma, Health Sciences Center, Oklahoma City, OK 73104, USA
4 - Department of Biochemistry and Molecular Biology, Bio21 Molecular Science and Biotechnology Institute, The University of Melbourne, Parkville, Victoria 3010, Australia

Correspondence to Michael W. Parker: *ACRF Rational Drug Discovery Centre, Biota Structural Biology Laboratory, St. Vincent's Institute of Medical Research, 9 Princes Street, Fitzroy, Victoria 3065, Australia.* mparker@svi.edu.au
http://dx.doi.org/10.1016/j.jmb.2013.11.020
Edited by I. B. Holland

Abstract

Cholesterol-dependent cytolysins (CDCs) are a large family of bacterial toxins that exhibit a dependence on the presence of membrane cholesterol in forming large pores in cell membranes. Significant changes in the three-dimensional structure of these toxins are necessary to convert the soluble monomeric protein into a membrane pore. We have determined the crystal structure of the archetypical member of the CDC family, streptolysin O (SLO), a virulence factor from *Streptococcus pyogenes*. The overall fold is similar to previously reported CDC structures, although the C-terminal domain is in a different orientation with respect to the rest of the molecule. Surprisingly, a signature stretch of CDC sequence called the undecapeptide motif, a key region involved in membrane recognition, adopts a very different structure in SLO to that of the well-characterized CDC perfringolysin O (PFO), although the sequences in this region are identical. An analysis reveals that, in PFO, there are complementary interactions between the motif and the rest of domain 4 that are lost in SLO. Molecular dynamics simulations suggest that the loss of a salt bridge in SLO and a cation–pi interaction are determining factors in the extended conformation of the motif, which in turn appears to result in a greater flexibility of the neighboring L1 loop that houses a cholesterol-sensing motif. These differences may explain the differing abilities of SLO and PFO to efficiently penetrate target cell membranes in the first step of toxin insertion into the membrane.

© 2013 Elsevier Ltd. All rights reserved.

Streptolysin O (SLO) belongs to a large family of pore-forming toxins called the cholesterol-dependent cytolysins (CDCs) [1–4]. It is produced by many strains of β-hemolytic group A, C and G streptococci. These human-specific pathogens are responsible not only for a variety of common infectious diseases including streptococcal sore throat (pharyngitis), rheumatic fever, scarlet fever and "school" sores (impetigo) but also for potentially life-threatening conditions such as toxic shock syndrome and "flesh-eating" infections such as necrotizing fasciitis [5]. SLO has been shown to be a key virulence factor of group A streptococci by preventing internalization of the bacteria into lyso-somes where they can be destroyed [6]. Recent studies suggest that SLO may be a multi-functional protein that has both pore-dependent and pore-independent functions [7–9].

SLO is 571 residues long but undergoes proteolytic cleavage by streptococcal proteases subsequent to secretion, removing an N-terminal region of about 70 residues [10–13]. The sequence of this N-terminal region does not align with any other CDC or other proteins. Secondary structure predictions suggest that this region, which we call domain 0, is unlikely to adopt any regular structure and does not affect toxic activity [14,15] but that it is critical for the SLO-mediated

translocation of *Streptococcus pyogenes* NAD-glyco-hydrolase into the cytoplasm of the host cell leading to an increase in cytotoxicity [8,16]. Electron microscopy studies reveal that SLO forms ring-like structures on erythrocyte membranes [17–22]. The formation of pores is a multi-staged process: first, binding to membranes in a monomeric form in a cholesterol-dependent manner followed by oligomerization and pore formation [21,23,24]. SLO has an 11-residue stretch of sequence (ECTGLAWEWWR), a signature sequence in CDCs, that is rich in tryptophan residues [11]. This undecapeptide has been shown to play a key role in the early stages of membrane insertion [3,4].

The first crystal structure of a CDC, perfringolysin O (PFO), revealed that CDCs consist of four domains (D1–D4) rich in β-sheet (see Fig. 1) [32]. Structure–function studies have highlighted the importance of D3 in providing the transmembrane spanning regions of the toxin and of D4 that takes part in the initial interactions with the membrane including direct interactions with cholesterol. The highly conserved undecapeptide sequence located in D4 adopted an extended loop structure. This loop, together with other loops at the base of D4 (L1 to L3), has been shown to provide the initial anchoring points for CDC interaction with the membrane surface, and this initial interaction somehow triggers changes in the remote D3 to start complete membrane penetration and pore formation [33,40,41]. Recent work has shown that cholesterol recognition occurs via a leucine-threonine motif in the L1 loop rather than through the undecapeptide loop [42].

We have crystallized and solved the structure of SLO. The SLO structure is similar to PFO [32,33] except that the CDC signature motif in D4 is sprung out from the body despite having an identical undecapeptide sequence with PFO. Molecular dynamics simulations of the crystal structures of SLO and PFO provide insights into the differing abilities of SLO and PFO to efficiently penetrate target cell membranes in the first step of toxin insertion into the membrane. The SLO crystal structure presented here will be of great value in rationally guiding the engineering of the toxin as a vaccine candidate [43], as an anti-cancer therapeutic [44] and as an adjuvant in stimulating inflammasome activity [45].

Crystal structure of SLO

One molecule was found in the asymmetric unit. Residues 103–571 (sequence numbering according to Ref. [11]) could be built into the electron density. Mass spectrometry of the SLO crystals revealed that D0 had cleaved from the full-length protein during the crystallization trial so that the first N-terminal residue was Glu103. The molecule is composed of four discontinuous domains and is rich in β-sheets (Fig. 1). D1 (residues 103–124, 161–249, 300–345 and 421–444) consists of a few α-helices and a

number of loops surrounding a core β-sheet, and D2 (residues 125–160 and 445–461) forms a three-stranded anti-parallel β-sheet; D3 (residues 250–299 and 346–420) is composed of a five-stranded anti-parallel β-sheet that is surrounded by the two transmembrane regions, TMH1 (residues 259–288) and TMH2 (residues 359–386), which adopt α-helical structure. D4 (residues 462–571) is folded into a compact β-sandwich with has four β-strands on each side of the sandwich. D2 is connected to D4 via a Ser-Gly linker (residues 462 and 463).

Dimers and monomers of CDCs

It has been suggested that CDCs may initially interact with membranes as dimers [46]. Head-to-tail dimers have been observed in the crystal structures of PFO, intermedilysin (ILY) and anthrolysin (ALO) [33,34,35], and PFO forms dimers in solution at high concentrations [47]. However, it is not clear whether such high concentrations would exist physiologically and, if so, the dimers would need to dissociate before oligomerization occurs as the toxin molecules are arranged head to head in the prepore and pore states [1–4]. In contrast to PFO, ALO and suilysin (SLY) have been shown to exist as monomers in solution [35,36].
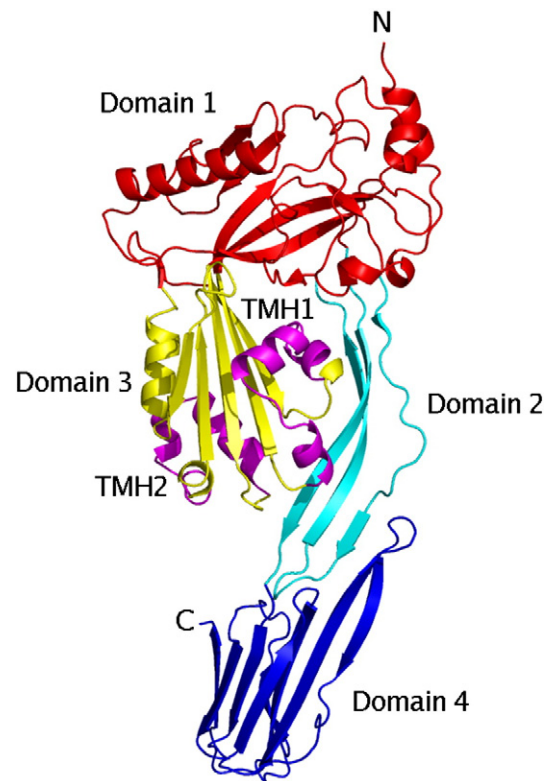

Fig. 1. (*legend on next page*)

When SLO is run under reducing conditions on a SDS-PAGE gel, it is present as monomers. A head-to-head non-covalent dimer is seen in the SLO crystals but the protein–protein interface, located between helix 1/first β-strand of D1 and the last two β-strands of D3, is small (540 Å^2 per monomer) and dominated by a few charged and polar residues (10 hydrogen bonds but no salt bridges). Thus, the "dimer" is likely to be a crystallographic artifact.

Comparison with other CDC structures

The overall structure of SLO is very similar to PFO (sequence identity of 66%) and other known CDC structures, but there are differences in domain orientations, in some of the loop regions (residues 167–173, 208–212, 239–244, 394–402 and 424–429) and in the N-terminus (Supplementary Information, Fig. S1a). A major difference is the orientation of D4 with respect to the rest of the molecule. For example, D4 is rotated by 17° from the long axis of the molecule in SLO compared to PFO. A previous study has shown that D4 rotation with respect to the long axis of the PFO molecule is coupled to D3 rotations despite there being no direct interactions between the two domains [33]. It was suggested that sufficient rotation of D4 would destroy all contacts at the D2–D3 interface leading to complete rotation of D3 away from the body of the molecule and thus allowing the release of the membrane inserting regions, TMH1 and TMH2, in D3. It is perhaps surprising that the detailed contacts are quite different between SLO and PFO. In SLO, there are 23 hydrogen bonding interactions between TMH1 and domains D1–D3 but only 7 of these are conserved in PFO. TMH2 has 8 interactions with D3 and none of these are conserved in PFO (Table S1).

Another prominent difference between SLO and the other CDCs is the conformation of the Trp-rich undecapeptide loop in D4 even though the amino acid sequences of the undecapeptide of PFO, SLO, ALO and SLY are strictly conserved (Fig. 2a). In SLO, the loop projects out from D4 although it makes a number of interactions with the rest of D4 including

Fig. 1. Crystal structure of SLO. Ribbon diagram with D1 in red, D2 in cyan, D3 in yellow and D4 in dark blue. The TMH1 and TMH2 regions are colored magenta. The gene for SLO was cloned from *S. pyogenes* as described previously [25]. Expression and purification were carried out as described previously for PFO [26]. An approximate yield of 10 mg/l of culture was obtained. SLO was stored at −20 °C in 1 mM ethylenediaminetetraacetic acid, 300 mM NaCl, 10 mM 4-morpholineethanesulfonic acid (Mes) (pH 6.5) and 10% (v/v) glycerol. For crystallization purposes, the protein was dialyzed against 1 mM ethylenediaminetetraacetic acid and 10 mM Mes (pH 6.5) and concentrated to 5 mg/ml. Prior to crystallization, DTT was added to a final concentration of 10 mM. The addition of DTT was necessary in order to exclusively obtain monomers. Without DDT, the protein solution consisted of monomers and dimers (judged by native SDS gel electrophoresis). Crystallization was performed using the vapor-diffusion hanging-drop method in 24-well Linbro culture plates (ICN, Biochemicals Inc., Ohio, USA). In initial crystallization screens, the "protein crystallization screen" [27] and the "Crystal Screen II" (Hampton Research, California, USA) were used at 22 °C. Crystallization drops were prepared by mixing 2 μl of protein with 2 μl of reservoir solution and were equilibrated against 1 ml of the reservoir solution. Small crystals appeared after 1 day in 18% (w/v) polyethylene glycol 8000 (Fluka Chemicals, Castle Hill, NSW, Australia), 20 mM CaCl$_2$ and 100 mM Mes (pH 6.5). The crystal size was improved by lowering the polyethylene glycol concentration to 10% (w/v) and by increasing the concentration of protein to 15 mg/ml. The crystals grew to maximal dimensions of 0.15 mm × 0.10 mm × 0.07 mm within 8 days. Some crystals were dissolved and analyzed on an Agilent Q-TOF for total molecular weight analysis and on an Orbitrap Elite for peptide mapping. The molecular weight analysis showed that the crystals were of a truncated form of SLO, suggesting that D0 had been removed and that this was confirmed by peptide mapping. Crystals for data collection were serially transferred to artificial mother liquor containing 5%, 10%, 15% and finally 20% (v/v) glycerol as cryo-protectant prior to freezing in a liquid nitrogen stream. The X-ray diffraction data were collected in-house at 100 K and recorded on a Rigaku R-AXIS IV++ imaging plate area detector (Rigaku, Japan) using a Rigaku MicroMax™ 007HF microfocus rotating anode generator (Rigaku, Japan) as an X-ray source. The data were processed using the program D*TREK [28]. A data set to a resolution of 2.1 Å was collected from a single crystal. D*TREK predicted that the crystal belonged to the space group $P2_1$ with unit cell dimensions of a = 46.2 Å, b = 85.3 Å, c = 81.2 Å and β = 92.1°. Assuming one molecule in the asymmetric unit, the V_M value for this crystal is 2.67 Å/Da with an estimated solvent content of 54% [29]. Molecular replacement was performed using the program MOLREP [30] in the CCP4 program suite [31]. The search model was the structure of PFO (PDB code: 1PFO). A solution could only be found if D4 was initially omitted from the search model. This is perhaps not surprising as D4 adopts different conformations with respect to the rest of the molecule in published CDC structures [32–36]. The location of D4 in SLO was found by performing another round of molecular replacement in which the solution obtained for D1 to D3 was fixed. The MOLREP R-factor after locating D1 to D3 was 46% and dropped to 42% after locating D4. After the first round of refinement, the values for R-factor and R_{free} were 36% and 30%, respectively. Alternate rounds of model building and refinement were performed with the program Coot [37], REFMAC5 [38] and PHENIX [39]. In total, 20 rounds of refinement were performed with the R-factor and R_{free} dropping after each round of refinement. Water molecules were built in during the last rounds of refinement. The final model yielded an R-factor and R_{free} of 22.2% and 26.4%, respectively. The Ramachandran plot showed that 99% of the residues were in the allowed regions with three residues as outliers (Asp171, Asp211 and Arg545). All residues are located in loop regions where the electron density is not well defined. The backbone of Ala368 forms hydrogen bonds with Arg413 and Ala364 (Ala368O to ArgNH1 and Ala368N to Ala364O). Data and refinement statistics are listed in Table S2. The coordinates for the SLO structure have been deposited in the Protein Data Bank (http://www.rcsb.org/pdb/) under the accession number 4HSC.
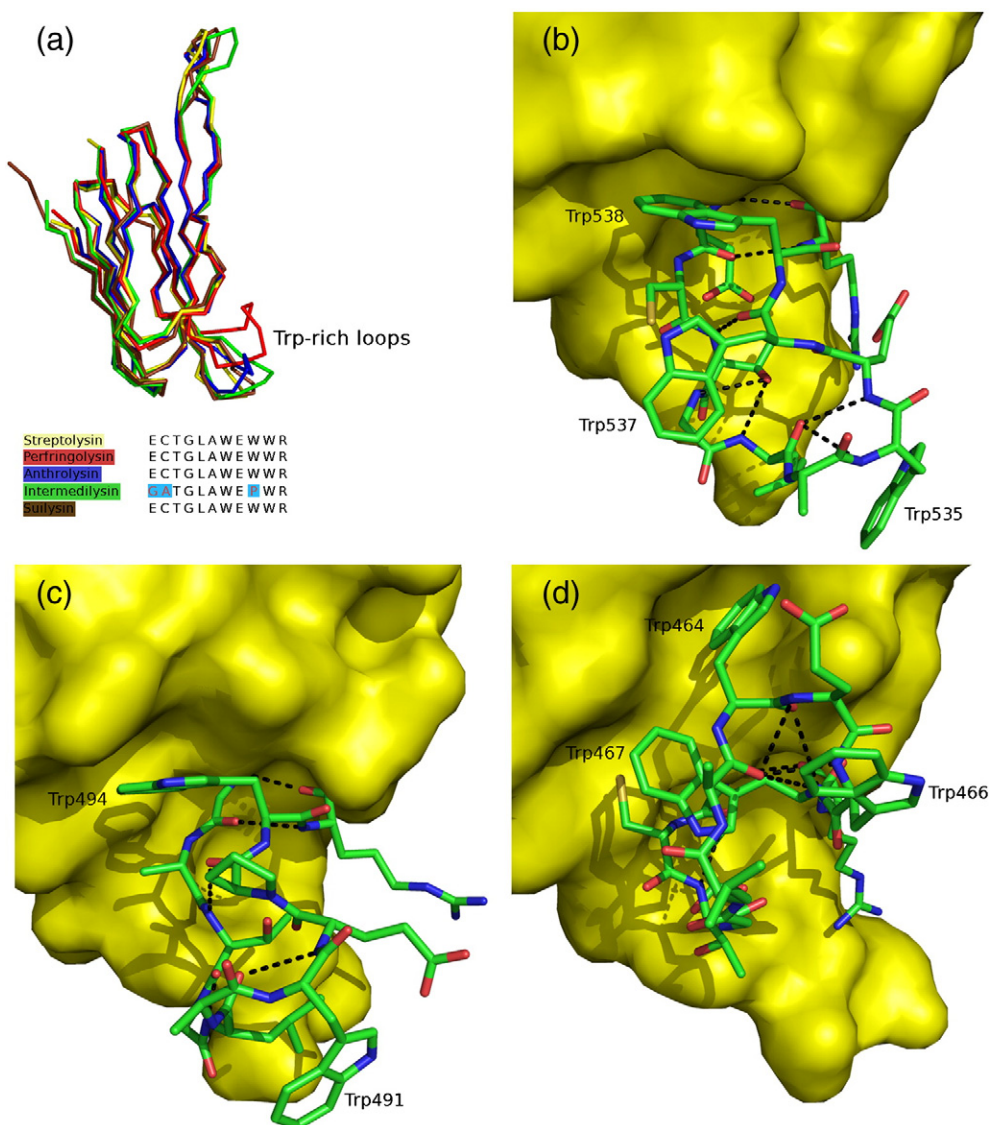
Fig. 2. Conformation of the Trp-rich loop. (a) Superposition of D4 of SLO (yellow) on PFO crystal form I (red), ILY molecule B (green), ALO molecule A (blue) and SLY (brown). A sequence alignment of the Trp-rich loop region of each toxin is shown below. (b–e) The Trp-rich loop interactions with D4 in various CDCs. D4 is shown as a yellow surface and the Trp-rich motif is shown as stick with standard atomic coloring. (b) SLO, (c) ILY and (d) PFO.

3 hydrogen bonds (Trp535 to Ala398 and to His40 via a water molecule, W537 to Thr245) and 12 van der Waals contacts (Fig. 2b). In PFO and ALO, this loop is curled up against one face of the β-sandwich, whereas in ILY and SLY, it adopts an extended conformation (Fig. 2a). The Trp-rich loop in SLO has a conformation most similar to SLY, and to a lesser extent ILY, although the extended loop in SLY is involved in extensive crystal contacts [36]; thus, it is difficult to make any definitive conclusions about it. In contrast, the SLO loop takes part in only two direct crystal contacts: the side chains of Trp535 and Trp537 are in hydrogen bonding distance of the main-chain carbonyls of Ala398 and Thr245 of a

neighboring molecule, respectively. The molecular dynamics simulations reported below suggest that the extended loop in SLO is a property of the molecule rather than being an artifact of crystallization. ILY is an atypical CDC with a variant undecapeptide sequence where the highly conserved cysteine is replaced by an alanine and the second conserved tryptophan residue is replace by a proline. It was suggested previously that Pro493 in ILY was responsible for the extended conformation of its undecapeptide (Fig. 2c) [34]. However, SLO retains a tryptophan residue in this position and the loop is still in an extended conformation (Fig. 2a). In PFO, Trp464 of the loop nestles into a hydrophobic
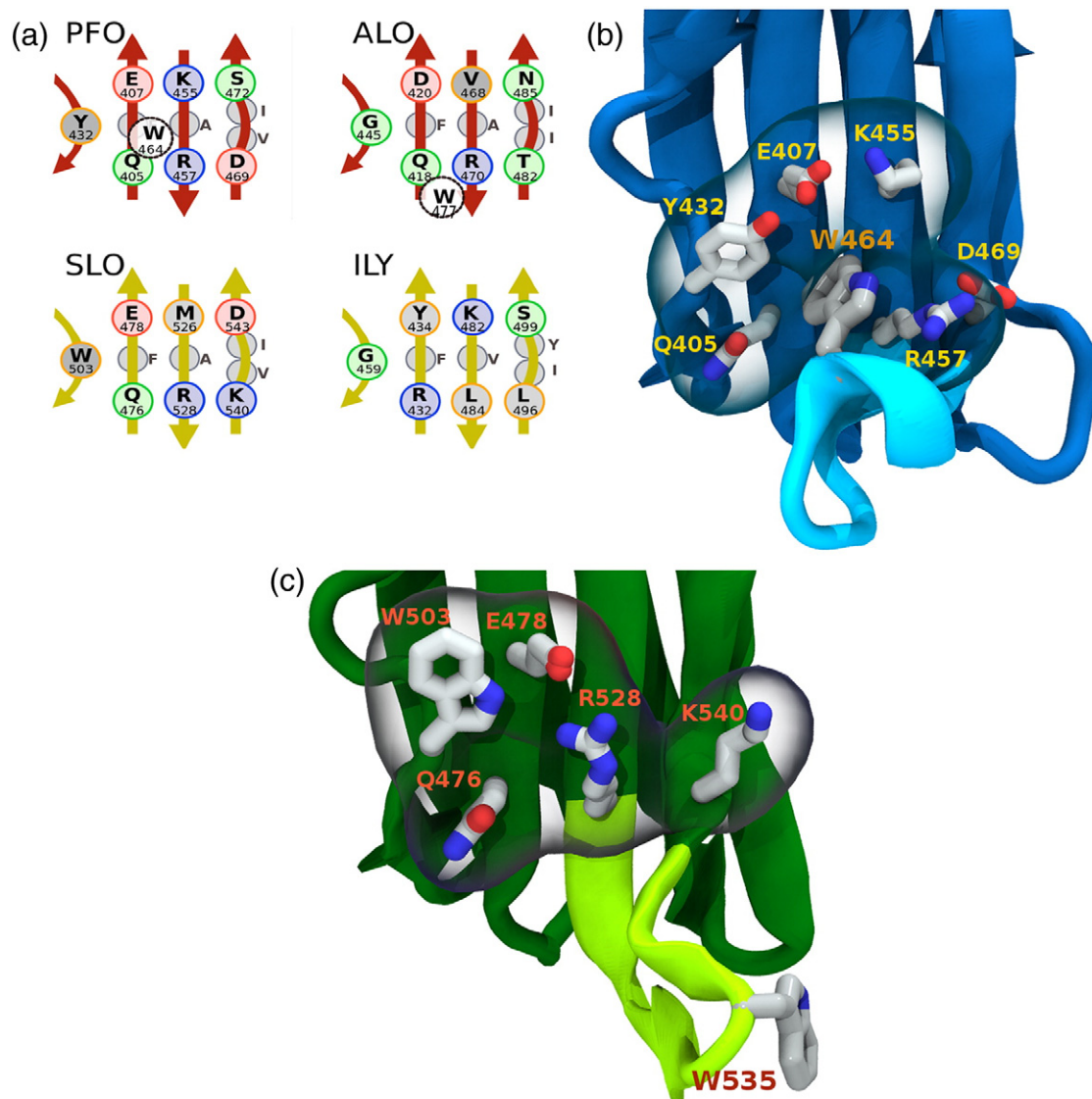
Fig. 3. Molecular dynamic simulations of SLO. (a) Diagrammatic view of the Trp-rich loop packing interfaces in PFO, ALO, SLO and ILY. Residues of the β-sheet (highlighted by the thick arrows) facing the D4 core are shown as gray circles and the nature of the other residues shown by different colored circles: red is negatively charged, blue is positively charged, green is polar and orange is hydrophobic. The hydrophobic pocket that the key stacking Trp from the Trp-rich loop occupies in PFO and ALO is shown as a white circle. (b) A representative shot from the molecular dynamics simulation of PFO D4 showing the conserved undecapeptide (in cyan) with Trp464 buried in the D4 interface. Salt bridges between Glu407 and Lys455 and between Arg457 and Asp469 help to create a well-defined pocket for Trp464. A "surface bubble" in light gray highlights key residues that form the binding pocket. (c) A representative shot from the molecular dynamics simulation of SLO D4 showing the extended conserved undecapeptide (in light green). Trp535 cannot bury into the D4 interface, like the equivalent residues in PFO, due to a salt bridge between Glu478 and Arg528. A "surface bubble" in light gray highlights key residues that block any potential binding pocket. To investigate the flexibility and dynamics of the Trp-rich and other D4 loops, we used models of D4 from the SLO and PFO (PDB code: 1M3I) crystal structures to undertake molecular dynamics simulation using NAMD 2.9 [49]. Models were initially solvated with TIP3 water under periodic boundary conditions of dimensions 48 Å × 48 Å × 64 Å. Charges were neutralized with NaCl for a total ionic concentration of 150 mM. Dynamic molecular modeling was conducted at a theoretical pH of 7.4. Two independent replicate simulations of each structure was performed for 250 ns (a total of 1000 ns simulation for both SLO and PFO models combined), at 310 K under NVT ensembles [a canonical ensemble where the number of moles (N), volume (V) and temperature (T) are conserved]. Trajectory snapshots were captured every 100 ps. The simulations were consolidated into their respective trajectories and analyzed for key residue interactions. All simulations were carried out in the absence of cholesterol and lipids.

pocket consisting of residues Trp467 and Tyr432 of the core β-sheet (Fig. 2d) but this pocket is not present in ALO and this is thought responsible for slightly different conformations of the Trp-rich loop in these two toxins. The hydrophobic pocket seen in PFO (Fig. 2d) is also absent in SLO (Fig. 2b), ILY (Fig. 2c) and SLY, thus providing an explanation of why the Trp-rich loop is extended in the latter toxins.

The cholesterol recognition motif in PFO was found to consist of Thr490 and Leu491 in the so-called L1 loop (residues 559–564 in SLO) of D4 [42]. The equivalent residues in SLO are Thr561 and Leu562, and this region superimposes very closely (r.m.s.d. of 0.95 Å over all atoms) with the equivalent region in PFO (Fig. S1a) reinforcing the importance of this region in recognizing cholesterol. The main-chain carbonyl of Leu562 is hydrogen bonded to Arg539, the last residue in the undecapeptide. A similar interaction takes place with Arg468 in PFO. The only sequence differences between PFO and SLO in L1 are Ser560 and Ser563 in the latter that are Thr489 and Tyr492 in the former.

As well as the Trp-rich membrane-sensing loop and L1 cholesterol-sensing loop, there are two other loops, L2 (residues 469–475 in SLO) and L3 (residues 505–509 in SLO), at the same end of the toxin molecule that might interact with the surface of the target membrane [40,48]. The conformation and sequence of the L2 loop is identical between SLO and PFO (Fig. S2b) with one exception: Gln470 in SLO is replaced by Ser399 in PFO. In contrast, the sequence of the L3 loop is different: Ser505, Ser508 and Pro509 in SLO are replaced by Asp434, Ala437 and His439, respectively, in PFO. However, despite the sequence variation, the loops in the two toxins adopt very similar conformations (Fig. S2c). Recently, other workers have found that replacing Asp434 with Ser in PFO decreased the amount of membrane cholesterol required for membrane binding whereas replacing Leu491 by Ser in the L1 loop increased the amount required [48]. Although SLO has the Asp-to-Ser replacement in L3, it does not have any obvious consequence for the three-dimensional structure in this region of the toxin. The work by Johnson _et al._ demonstrates the importance of the D4 distal loops in membrane binding and how sensitive to subtle changes they can be [48].

Molecular simulations of SLO and PFO domain 4

The D4 interface abutting the Trp-rich loop is quite varied between CDCs as shown in Fig. 3a. The significance of the sprung out Trp-rich loop in SLO was further explored with molecular dynamics simulations. Two replicate 250-ns fully solvated molecular dynamics simulations of D4 from SLO and PFO were performed to help identify how key structural differences might affect the undecapeptide conformation. Our simulations suggested that the D4-undecapeptide

loop interface appeared to stabilize the curled undecapeptide conformation in PFO predominantly due to the contact of Trp464 from the loop being nestled in a cluster of residues, namely Gln405, Glu407, Lys455 and Arg457, and also stabilizing a cation–pi interaction between Arg457 and Trp464 (Fig. 3b). Importantly, a salt bridge interaction between Arg457 and the adjacent Asp469 in PFO pulls the arginine residue aside allowing a better interaction of Trp464 within the residue cluster. The simulations also suggested that the SLO undecapeptide, in contrast to PFO, remains largely in the extended conformation, probably due to the inability of the equivalent tryptophan at residue 535 to interact with the analogous D4 interface and Arg528 (Fig. 3c). The simulations indicate that Arg528 (equivalent to PFO Arg457) is unable to form a salt bridge as it does in PFO (with Asp469) since the equivalent residue is a lysine (SLO Lys540). Instead, Arg528 in SLO interacts predominantly with Gln476 and Glu478, effectively blocking any potential interaction of Trp535 at that interface. An alternate cation–pi interaction in SLO appears between Arg528 and Trp538 to further stabilize the extended form of the undecapeptide.

One consequence of the curled conformation of the PFO undecapeptide loop, mediated by the interaction of Trp464 with the D4 interface, is that the two residues found to be important for cholesterol detection in the membrane, Thr490 and Leu491 on loop L1, are held in a relatively stable conformation due to hydrogen bond interactions between Arg468 and the L1 backbone [50]. The extended undecapeptide conformation of SLO appears to allow more flexibility of the conserved Arg consequently allowing more flexibility of the L1 loop. This is supported by simulation measurements of the positional r.m.s.d. of the C^α of this threonine/leucine pair that is 2.2 Å with a standard deviation of 0.9 Å in the PFO model and that is 3.5 Å with a standard deviation of 2.1 Å in the SLO model. The relative additional flexibility of the L1 loop of SLO may provide insight into the observation that the PFO Trp-rich loop penetrates the membrane more effectively than SLO (R.K.T., unpublished results). The orientation of the conserved L1 leucine is certainly unusual as it projects as a sort of "hydrophobic finger" at one corner of D4. Such hydrophobic projections are unexpected as typically hydrophobic residues of soluble proteins tend to cluster internally as part of hydrophobic cores structures [51].

Concluding remarks

The structure determination of SLO reveals a strong similarity of its fold to PFO suggesting that many of the structure–function studies performed on the latter are directly relevant to understanding SLO activity. Importantly, we found three features in the membrane-sensing domain (D4) that differed from the much better studied PFO, which might modulate

how SLO interacts with membranes. Firstly, the Trp-rich loop is extended in SLO, and secondly, simulations suggest that there is an increased flexibility in the cholesterol-sensing L1 loop; thirdly, the L3 loop has a serine replacement that has been shown in PFO to significantly affect membrane cholesterol sensing. Recent work suggesting that the Trp-rich loop of SLO does not penetrate the membrane nearly and PFO may be related to the increased flexibility of the membrane proximal loops in D4.

Supplementary data to this article can be found online at http://dx.doi.org/10.1016/j.jmb.2013.11.020.

References

[1] Tweten RK, Parker MW, Johnson AE. The cholesterol-dependent cytolysins. In: van der Goot FG, editor. Pore-forming toxins. Heidelberg, Germany: Springer; 2001. p. 1–14.

[2] Parker MW, Feil SC. Pore-forming proteins: from structure to function. Prog Biophys Mol Biol 2005;88:91–124.

[3] Tweten RK. Cholesterol-dependent cytolysins, a family of versatile pore-forming toxins (minireview). Infect Immun 2005;73:6199–209.

[4] Hotze EM, Tweten RK. Membrane assembly of the cholesterol-dependent cytolysin pore complex. Biochim Biophys Acta 2012;1818:1028–38.

[5] Cunningham MW. Pathogenesis of group A streptococcal infections. Clin Microbiol Rev 2000;13:470–511.

[6] Håkansson A, Bentley CC, Shakhnovic EA, Wessels MR. Cytolysin-dependent evasion of lysosomal killing. Proc Natl Acad Sci USA 2005;102:5192–7.

[7] Logsdon LK, Håkansson AP, Cortés G, Wessels MR. Streptolysin O inhibits clathrin-dependent internalization of group A *Streptococcus*. mBio 2011;2. http://dx.doi.org/10.1128/mBio.00332-10.

[8] Madden JC, Ruiz N, Caparon M. Cytolysin-mediated translocation (CMT): a functional equivalent of type III secretion in Gram-positive bacteria. Cell 2001;104:143–52.

[9] Magassa N, Chandrasekaran S, Caparon MG. *Streptococcus pyogenes* cytolysin-mediated translocation does not require pore formation by streptolysin O. EMBO Rep 2010;5:400–5.

[10] Kehoe MA, Timmins KN. Cloning and expression in *Escherichia coli* of the streptolysin O determinant and demonstration of the absence of substantial homology with determinants from other thiol-activated toxins. Infect Immun 1984;43:804–10.

[11] Kehoe MA, Miller L, Walker JA, Boulnais GJ. Nucleotide sequence of the streptolysin O (SLO) gene: structural homologies between SLO and other membrane-damaging thiol-activated toxins. Infect Immun 1987;55:3228–32.

[12] Gerlach D, Kohler W, Gunther E, Mann K. Purification and characterization of streptolysin O secreted by *Streptococcus equisimilis* (group C). Infect Immun 1993;61:27227–31.

[13] Bhakdi S, Bayley H, Valeva A, Walev I, Walker B, Kehoe M, et al. Staphylococcal alpha-toxin, streptolysin-O, and *Escherichia coli* hemolysin: prototypes of pore-forming bacterial cytolysins. Arch Microbiol 1996;165:73–9.

[14] Weller U, Miller L, Messner M, Palmer M, Valeva A, Tranum-Jensen J, et al. Expression of active streptolysin O in *Escherichia coli* as a maltose-binding-protein–streptolysin-O fusion protein. The N-terminal 70 amino acids are not required for hemolytic activity. Eur J Biochem 1996;236:34–9.

[15] Meehl MA, Caparon MG. Specificity of streptolysin O in cytolysin-mediated translocation. Mol Microbiol 2004;52:1665–76.

[16] Bricker AL, Cywes C, Ashbaugh CD, Wessels MR. NAD$^+$-glycohydrolase acts as an intracellular toxin to enhance the extracellular survival of group A streptococci. Mol Microbiol 2002;44:257–69.

[17] Dourmashkin RR, Rosse WF. Morphologic changes in the membranes of red blood cells undergoing hemolysis. Am J Med 1966;41:699–700.

[18] Duncan JL, Schlegel R. Effect of streptolysin O on erythrocyte membranes, liposomes, and lipid dispersions. A protein-cholesterol interaction. J Cell Biol 1975;67:160–74.

[19] Rosenqvist E, Michaelsen TE, Vistnes AI. Effect on streptolysin O on egg lecithin/cholesterol vesicles. Biochim Biophys Acta 1980;600:91–102.

[20] Buckingham L, Duncan JL. Approximate dimensions of membrane lesions produced by streptolysin S and streptolysin O. Biochim Biophys Acta 1983;729:115–22.

[21] Bhakdi S, Tranum-Jensen J, Sziegoleit A. Mechanism of membrane damage by streptolysin-O. Infect Immun 1985;47:52–60.

[22] Sekiya K, Satoh R, Danbara H, Futaesaku Y. A ring shaped structure with a crown formed by streptolysin O on the erythrocyte membrane. J Bacteriol 1993;175:5953–61.

[23] Niedermeyer W. Interaction of streptolysin-O with biomembranes: kinetic and morphological. Toxicon 1985;23:425–39.

[24] Hugo F, Reichwein J, Arvand M, Kraemer S, Bhakdi S. Use of a monoclonal antibody to determine the mode of transmembrane pore formation by streptolysin O. Infect Immun 1986;54:641–5.

[25] Giddings KS, Johnson AE, Tweten RK. Redefining cholesterol's role in the mechanism of the cholesterol-dependent cytolysins. Proc Natl Acad Sci USA 2003;100:11315–20.

[26] Shepard LA, Heuck AP, Hamman BD, Rossjohn J, Parker MW, Ryan KR, et al. Identification of a membrane-spanning domain of the thiol-activated pore-forming toxin *Clostridium perfringens* perfringolysin O: an alpha-helical to beta-sheet transition identified by fluorescence spectroscopy. Biochemistry 1998;37:14563–74.

[27] Zeelen JP, Hiltunen JK, Ceska TA, Wierenga RK. Crystallisation experiments with 2-enoyl-CoA hydratase, using an automated "fast screening" crystallization protocol. Acta Crystallogr Sect D Biol Crystallogr 1994;50:443–7.

[28] Plugrath JW. The finer things in X-ray diffraction data collection. Acta Crystallogr Sect D Biol Crystallogr 1999;55:1718–25.

[29] Matthews BW. Solvent content of protein crystals. J Mol Biol 1968;33:491–7.

[30] Vagin A, Teplyakov A. MOLREP, an automated program for molecular replacement. J Appl Crystallogr 1997;30:1022–5.

[31] Winn MD, Ballard CC, Cowtan KD, Dodson EJ, Emsley P, Evans PR, et al. Overview of the CCP4 suite and current developments. Acta Crystallogr Sect D Biol Crystallogr 2011;67:235–42.

[32] Rossjohn J, Feil SC, McKinstry WJ, Tweten RK, Parker M. Structure of a cholesterol-binding, thiol-activated cytolysin and a model of its membrane form. Cell 1997;89:685–92.

[33] Rossjohn J, Polekhina G, Feil SC, Morton CJ, Tweten RK, Parker MW. Structures of perfringolysin O suggest a pathway for activation of cholesterol-dependent cytolysins. J Mol Biol 2007;367:1227–38.

[34] Polekhina G, Giddings KS, Tweten RK, Parker MW. Insight into the action of the superfamily of cholesterol-dependent cytolysins from studies of intermedilysin. Proc Natl Acad Sci USA 2005;102:600–5.

[35] Bourdeau RW, Malito E, Chenal A, Bishop BL, Musch MW, Villereal EBC, et al. Cellular functions and X-ray structure of anthrolysin O, a cholesterol-dependent cytolysin secreted by *Bacillus anthracis*. J Biol Chem 2009;284:14645–56.

[36] Xu L, Huang B, Du H, Zhang XC, Xu J, Rao Z. Crystal structure of cytotoxin protein suilysin from *Streptococcus suis*. Protein Cell 2010;1:96–105.

[37] Emsley P, Cowtan K. Coot: model-building tools for molecular graphics. Acta Crystallogr Sect D Biol Crystallogr 2004;60:2126–32.

[38] Murshudov GN, Vagin AA, Dodson EJ. Refinement of macromolecular structures by the maximum-likelihood method. Acta Crystallogr Sect D Biol Crystallogr 1997;53:240–55.

[39] Adams PD, Grosse-Kunstleve RW, Hung LW, Ioerger TR, McCoy AJ, Moriarty NW, et al. PHENIX: building new software for automated crystallographic structure determination. Acta Crystallogr Sect D Biol Crystallogr 2002;58:1948–54.

[40] Ramachandran R, Heuck AP, Tweten RK, Johnson AE. Structural insights into the membrane-anchoring mechanism of a cholesterol-dependent cytolysin. Nat Struct Mol Biol 2002;9:823–7.

[41] Soltani CE, Hotze EM, Johnson AE, Tweten RK. Structural elements of the cholesterol–dependent cytolysins that are responsible for their cholesterol-sensitive membrane interactions. Proc Natl Acad Sci USA 2007;104:20226–31.

[42] Farrand AJ, LaChapelle S, Hotze EM, Johnson AE, Tweten RK. Only two amino acids are essential for cytolytic toxin recognition of cholesterol at the membrane surface. Proc Natl Acad Sci USA 2010;107:4341–6.

[43] Chiarot E, Faralla C, Chiappini N, Tuscano G, Falugi F, Gambellini G, et al. Targeted amino acid substitutions impair streptolysin O toxicity and group A *Streptococcus* virulence. mBio 2013;4:e00387–003912.

[44] Yang WS, Park S-O, Yoon A-R, Yoo JY, Kim MK, Yun C-O, et al. Suicide cancer gene therapy using pore-forming toxin, streptolysin O. Mol Cancer Ther 2006;5:1610–9.

[45] Keyel PA, Roth R, Yokoyama WM, Heuser JE, Salter RD. Reduction of streptolysin O (SLO) pore-forming activity enhances inflammasome activation. Toxins 2013;5:1105–18.

[46] Gilbert RJ. Inactivation and activity of cholesterol-dependent cytolysins: what structural studies tell us. Structure 2005;13:1097–106.

[47] Solovyoya AS, Noellmann M, Mitchell TJ, Byron O. The solution structure and oligomerization behaviour of two bacterial toxins: pneumolysin and perfringolysin O. Biophys J 2004;87:540–52.

[48] Johnson BB, Moe PC, Chang Y, Wang D, Rossi K, Trigatti BL, et al. Modifications in perfringolysin O domain 4 alter the threshold of cholesterol concentration required for binding. Biochemistry 2012;51:3373–82.

[49] Phillips JC, Braun R, Wang W, Gumbart J, Tajkhorshid E, Villa E, et al. Scalable molecular dynamics with NAMD. J Comput Chem 2005;26:1781–802.

[50] Dowd KJ, Farrand AJ, Tweten RK. The cholesterol-dependent cytolysin signature motif: a critical element in the allosteric pathway that couples membrane binding to pore assembly. PLoS Pathog 2012;8:e1002787.

[51] Pace CN, Shirley BA, McNutt M, Gajiwala K. Forces contributing to the conformational stability of proteins. FASEB J 1996;10:75–83.